Hydrographic characteristics of the Indian sector of the Southern Ocean

P. V. Shirodkar*, Y. K. Somayajulu, Y. V. B. Sarma and R. Vijayakumar

National Institute of Oceanography, Dona Paula, Goa 403 004, India

Oceanographic studies in the Indian sector of the Southern Ocean (58–61°S and 30–40°E) carried out during December 1995 and March 1996 indicate a 3-layer structure typical of summer in the oceanic domain south of the Antarctic Polar Front. The upper 300 m water column consists of three distinctive thermohaline characteristics. The surface layer (50 m) of summer surface water formed by seasonal warming with temperatures (0–2°C) and low salinity (< 33.8 PSU), the intermediate layer (50–150 m) of winter reminiscent water with negative temperatures (0 to –2°C) and moderate salinity (33.8–34.3 PSU) and the deeper layer (below 150 m) of Circumpolar Deep Watermass (CDW) with positive temperatures (0–2° C) and higher salinity (34.3–34.8 PSU). The influence of the strong Antarctic Divergence between the east and west drifts is noticed at 61°S, 34°E marked by phytoplankton and zooplankton patches.

The dissolved oxygen (DO) shows high concentrations (7.6 to >8.0 ml l^{-1}) in the upper layer. These higher levels of DO sometimes extend down to the intermediate layer and gradually decrease further downwards. The observed low temperature and high DO in the subsurface water (50–75 m) are typical signatures of Antarctic Winter Watermass (AWW) formed during winter. Calcium, magnesium and boron show significant spatial variations with higher values of Ca and Mg along 59°S and 60°S relative to 61°S. Ca exhibits large variations (398–421 mg kg^{-1} while Mg shows least variations with concentrations close to the average value for normal sea water (1294 mg kg^{-1}). Boron depicts high values along 59°S and 61°S compared to 60°S, with higher values in the subsurface layer (25–75 m) which are attributed to biological characteristics and the frontal systems in the region.

Phytoplankton cell counts remain high (between 1.92 and 22.9 × 10^4 per litre) while zooplankton biomass shows variations from 9.8 to 303.62 ml 100 m^{-3}. A marked drop of both phytoplankton and zooplankton in the region of krill swarm (between 60°40'–61°13'S and 33° 34'–34°14'E), however, indicates active feeding by the latter on the planktonic communities.

THE Southern Ocean is characterized by large seasonal variability in its environmental conditions which influence the global climate. This has led to a growing interest in the exploration of the Southern Ocean to understand various physical, chemical and biological processes and their driving mechanisms operating in this region. Compared to the Atlantic and Pacific sectors of the Southern Ocean, its Indian Ocean sector has remained largely unexplored.

The area under investigation lies in the vicinity of the Antarctic Divergence Zone. The oceanic frontal systems in the Indian Ocean sector of the Southern Ocean have been described in detail by several researchers[1–7]. Lutjeharms[7] described in detail the nature and geographic distribution of major oceanic fronts south of Africa. The circulation south of 52°S extending up to 60°E corresponds to the eastern boundary of the Weddell Gyre[8]. This is consistent with the results of Fine Resolution Antarctic Model (FRAM)[9].

The present study on the physical, chemical and biological characteristics of waters in the region between

*For correspondence. (e-mail: ocean@bcgoa.ernet.in)

58°–61°S and 30°–40°E was carried out during the Indian Antarctic Krill Expedition on-board FORV *Sagar Sampada* from December 1995 to March 1996 (Figure 1). This expedition was aimed at exploiting the marine living resources in the Antarctic region and the stations for hydrographic sampling are broadly grouped into three zonal sections corresponding to 59°, 60°, 61°S latitudes, respectively as shown in Figure 1.

Materials and methods

A total of 90 sea water samples were collected from the upper 300 m water column from 16 stations (Figure 1) in the region (58 to 61.3°S and 30 to 40°E) at standard depths (surface, 50, 100, 150, 200, 250 and 300 m) using Sea-Bird CTD Rossette system provided with Niskin samplers. The collected samples were preserved in the deep freeze for analysis of major elements (such as calcium, magnesium and boron) at the shore laboratory. Temperature, salinity and dissolved oxygen (DO) data (after calibration) were obtained from the CTD on-board the ship. The calibration of CTD DO values was done

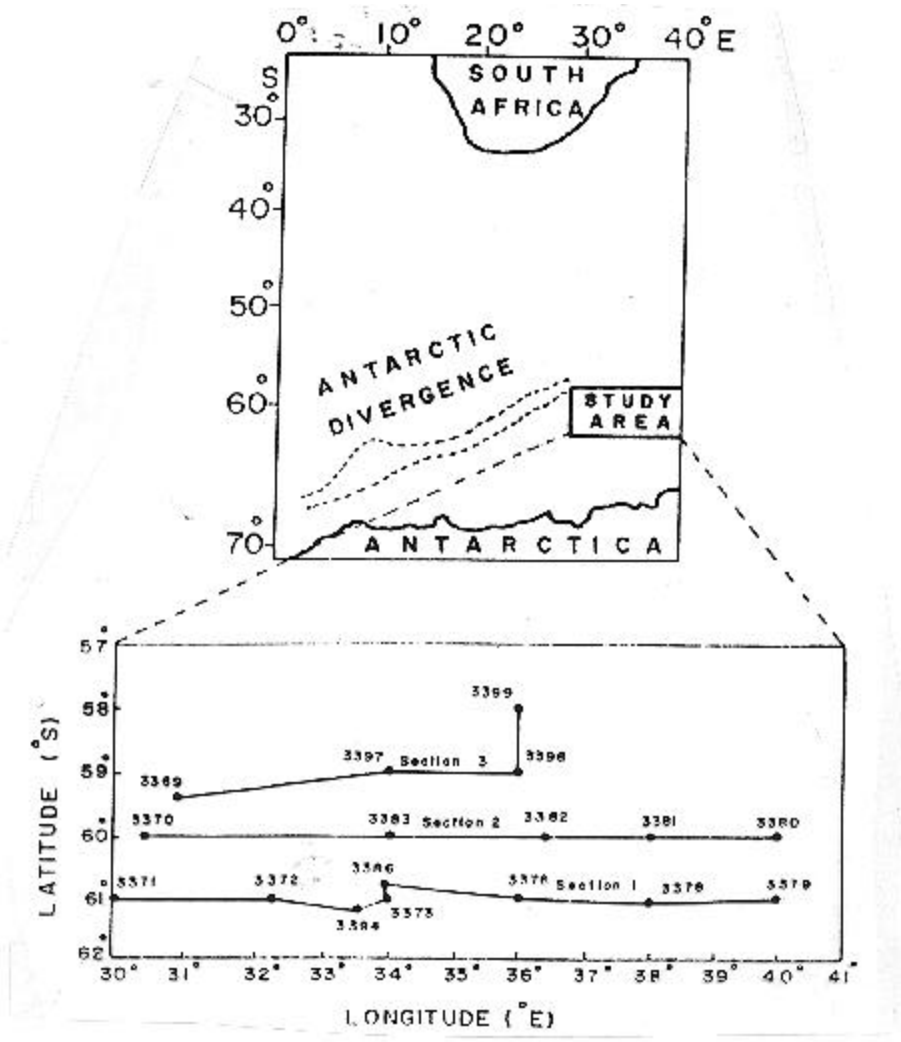

Figure 1. Study area showing Antarctic Divergence region (Inset: station locations; shaded area indicates potential region of krill

krill swarms).

using the relation obtained by the analysis of sea water samples following Winklers' titration method. The correlation of CTD DO values and the values obtained through Winklers' titration method gave the following equation:

$$DO_{Wink} = DO_{CTD} * 1.184175 + 0.430365,$$

with correlation coefficient, $r = 0.99$. The above relation was used for correcting the CTD DO values. The analyses of calcium and magnesium were carried out by the method of Culkin and Cox[10] and of boron by the spectrophotometric method of Hatcher and Wilcox[11].

In order to investigate phytoplankton and zooplankton distributions and their relation to krill, Bongo net and conical HT net/IOSN were operated for surface and vertical tows. Samples were collected at all the 16 stations by vertical hauls from 200 m to the surface using the Bongo net (60 cm mouth diameter, mesh size 40 m m) attached with a flow meter. The samples were fixed in 5% formaldehyde and the biomass was determined by the volume displacement method and expressed as ml/100 m^3 of water filtered. Major zooplankton taxa were sorted out from aliquots (25%) and species were identified wherever possible. The number of organisms was calculated for the whole sample and computed for 100 m^3. Percentage compositions of various zooplanktonic groups were calculated.

For enumeration of phytoplankton cells, the surface sea water samples were collected using Niskin samplers and transferred to 500 ml plastic bottles. The samples were preserved in Lugol's iodine and buffered formaldehyde solution. The phytoplankton cells were taxonomically identified and counted in Sedgwick Rafter counter cell using Olympus BH microscope.

Results and discussion

A marginal eastward (30 to 40°E) and considerable northward (61 to 59°S) increase of temperature is noticeable at the surface. While the surface temperatures varied from 0.85 to 1.65°C along 61°S, the corresponding variation in temperature for 60°S and 59°S are 1.32 to 1.80°C and 1.05 to 2.46°C, respectively (Figure 2*a*). An important feature of the vertical thermal structure is the occurrence of a negative temperature (–0.03 to
–1.58°C) layer of about 60–80 m thickness in the depth range 50–150 m. In this layer, the thermal structure reveals the presence of several eddy features discernible in the form of closed contours. Below 150 m, isotherms show a wavy pattern with a prominent peak around 34°E along 61°S. Below the negative temperature layer, a gradual increase of temperature with depth is found up to 300 m, where the values range between 1.4 and 1.8°C.

The spatial distribution of temperature at four levels, viz. surface, 50 m, 100 m, 200 m is shown in Figure 3*a*. The sea surface temperature (SST) varied between 1 and 2.2°C with a warm core around 59°S, 35°E. SST in the western region exhibits an eastward increase, while in the rest of the region a gradual northward increase is noticed. At 50 m depth, isotherms indicate the presence of cold polar waters with temperatures ranging from 0.8 to 1.2°C with relatively cold water occurring in the south-western region. At 100 m depth, subzero temperatures with a core temperature of –1.6°C were noticed around 61°S, 30°E. At 200 m, temperatures are positive and depict negligible east-west variation. However, a warm core cell is evident between 33° and 34°E. In general, the spatial distribution of temperature is characterized by cold intermediate layer trapped between relatively warm upper and lower layers.

The vertical distributions of salinity along the three zonal sections are shown in Figure 2*b*. A predominant upward lifting of the isohalines along 61°S is noticed around 33°E in the vicinity of Antarctic Divergence[7]. Further eastward a gradual spreading of isohalines is noticed. Salinity varies between 33.0 and 34.7 PSU in the upper 300 m, and increases gradually with depth. The surface salinity varies between 33.0 and 34.0 PSU with lower values on the western side and higher values towards north-east. While the pattern remains the same at 50 m, variability is seen between 33.77 and 33.94 PSU in the same regions as at the surface. The salinity distribution at 100 m and 200 m shows variations between 33.98–34.20 PSU and 34.30–34.56 PSU, respectively, with a gradual decrease towards north. The high saline waters in the subsurface (100–200 m depth) are probably due to upwelling. The lateral mixing of ambient waters with cold Antarctic waters modifies the temperature and salinity characteristics to different degrees.

The density (s_t) distribution along 61°S shows strong divergence with an upward tilt of isopycnals (isolines of s_t) around 33°E (Figure 2*c*). A similar but less pronounced upward tilt of isopycnals below 150 m is centred at 37.5°E. A reverse pattern is present in 60°S at corresponding longitudes. The distribution of s_t closely resembles salinity, indicating the latter's influence on the density of the water column. s_t gradually increased downwards from 27.1 near the surface to 27.7 at 300 m. At the sea surface, s_t varies between 27.0 and 27.15 (Figure 3*c*) while at 50 m, it varies between 27.37 and 27.47. The cells of maximum density at both 50 and 100 m levels occurred around the same location, indicating persistence of the subsurface feature associated with geostrophic upwelling. The density gradually decreased towards east. At 200 m, the isopycnals show variations between 28.49 and 28.63 with cells of higher values corresponding to the same location as at 100 m. The phenomenon of geostrophic upwelling can be substantiated when the vertical density structure is examined in conjunction with the density flux function (t), which is an indicator of the nature of mixing of water[12,13]. At the places where the isolines of s_t and t intersect, vertical mixing (Ekman pumping) is predominant and when both are parallel, it indicates lateral mixing of waters. Along the three sections, the isolines of t (dashed lines in Figure 2*c*) resemble the corresponding vertical thermal structure along these sections. The upper 150 m region is characterized by closed cells followed by upward tilt of isolines below this depth. A strong vertical mixing generated by eddy circulation is evident in the t distribution showing steep vertical intersection of isopycnals around 31 and 35°E (Figure 2*c*).

Mean temperature profiles along 61, 60 and 59°S sections (Figure 4*a*) highlight three distinct layers of the water column. The near surface layer having a thickness of about 50 m with positive temperatures (0–2°C) and lower salinity (< 33.8 PSU); the intermediate layer (50–150 m) with negative temperatures (–1.6 to –0.2) and a salinity in the range 33.8–34.3 PSU; the third layer (150–300 m) characterized by positive temperatures
(0–2°C) and relatively higher salinity in the range 34.3–34.8 PSU. s_t values for these waters correspond to < 27.20, 27.2–27.6 and 27.5–27.78 in the three layers, respectively. The T–S indices and s_t interval reveal that the surface layer is formed through summer warming whereas the intermediate layer consists of waters formed during the preceding winter and the lower layer is the characteristic of Circumpolar Deep Watermass (CDW). The T–S scatter (Figure 4*b*) indicates wider variations

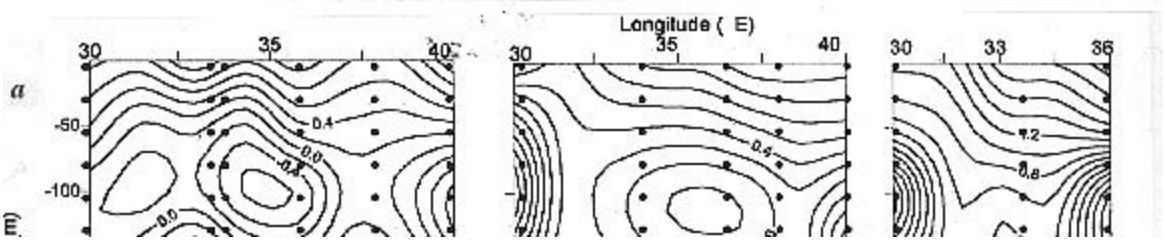

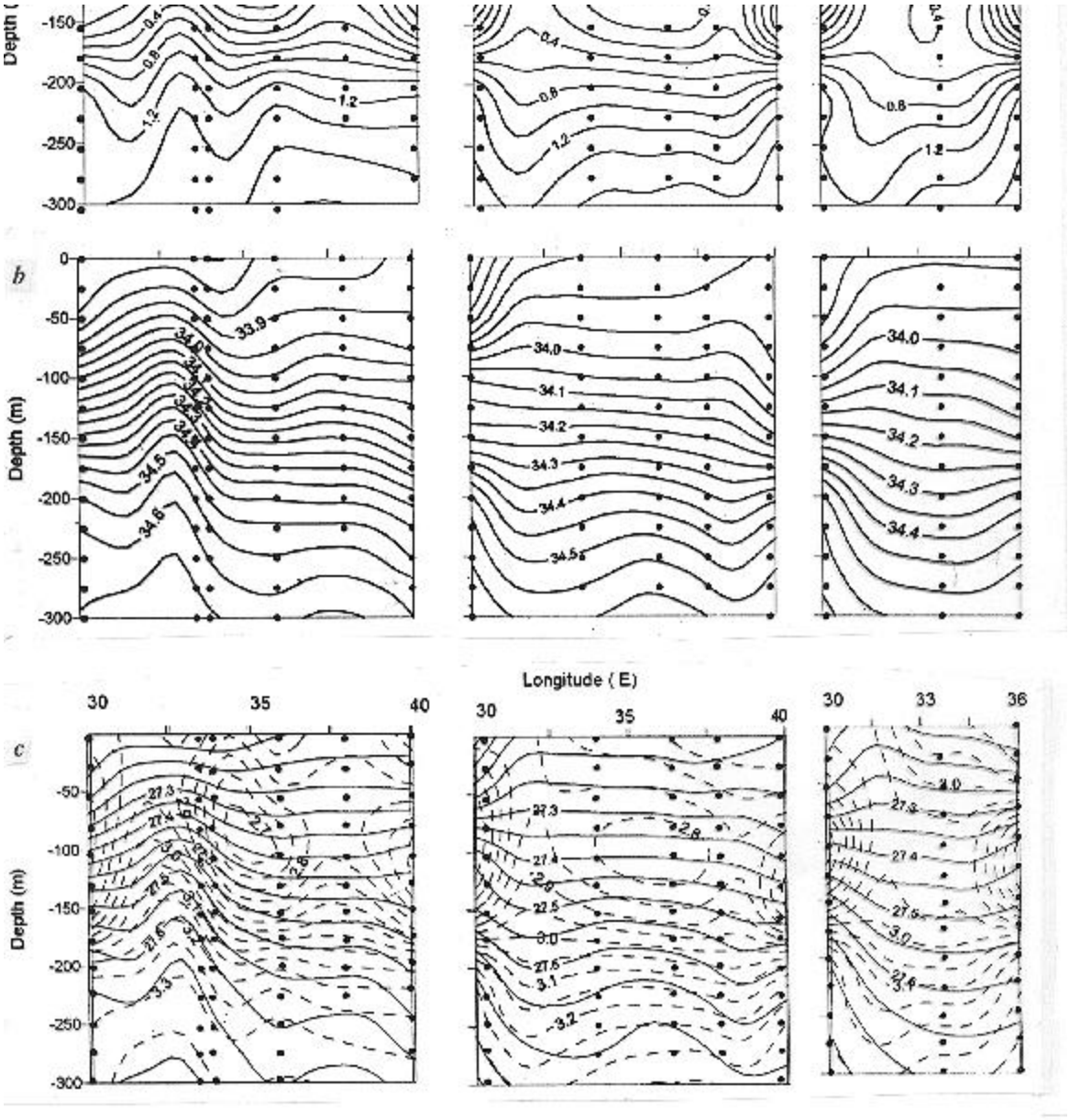

Figure 2. Vertical sections along 61, 60 and 59°S of *a*, Temperature (°C); *b*, Salinity (PSU); *c*, Density (σ_t) (kg m^{-3}) and Density Flux Function, τ.

of temperature compared to salinity in layers 1 and 2. The depth of occurrence and the thickness of sub zero temperature layer gradually increase towards north. Similarly, the mean T–S scatter indicates large spatial

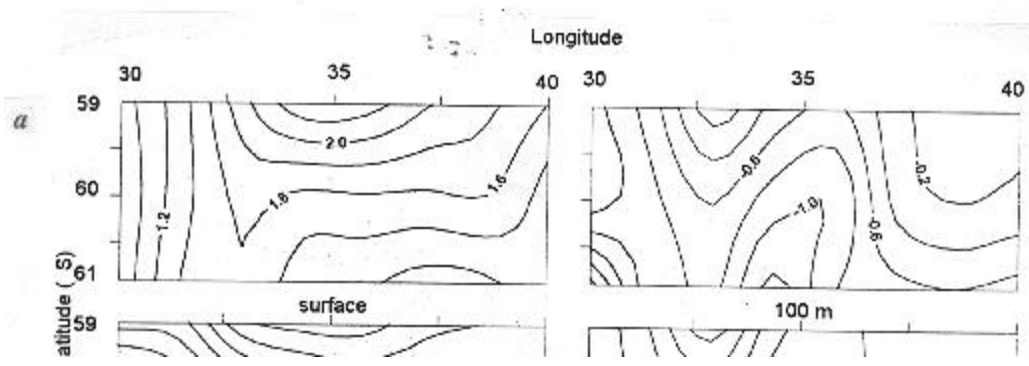

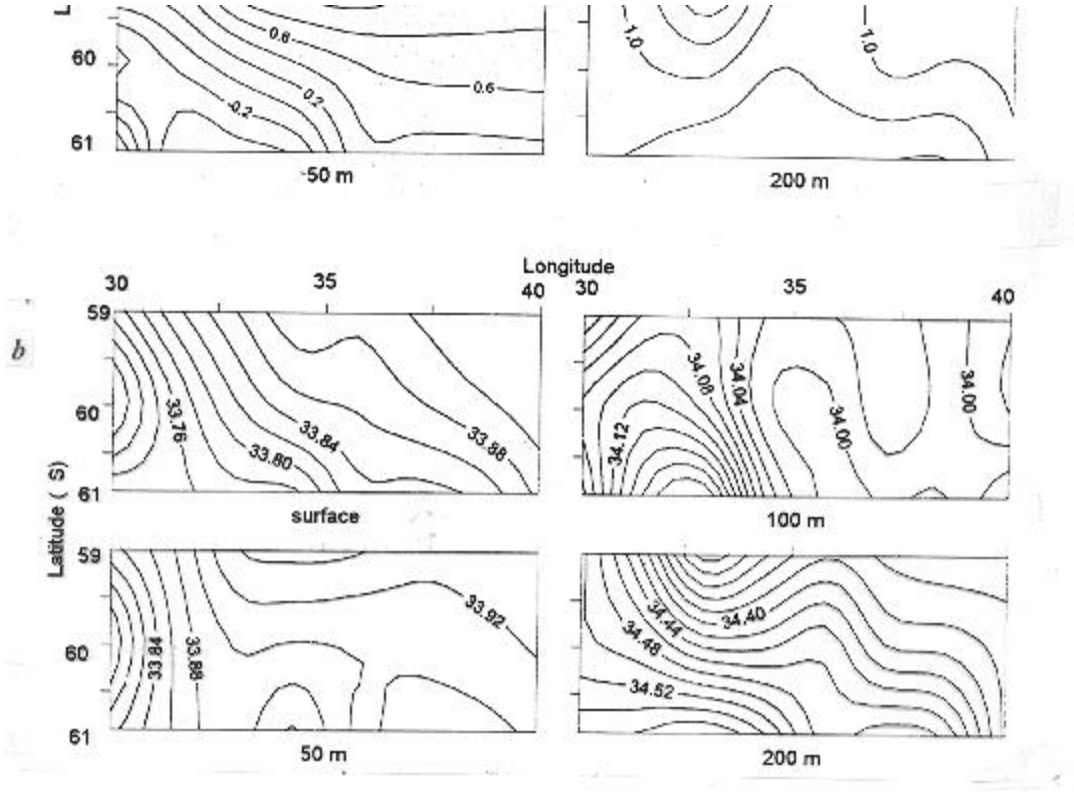

Figure 3 *a*, *b*. Spatial distribution of *a*, Temperature (°C); *b*, Salinity (PSU).

variability among the three sections. Salinity range of the intermediate layer for 61°S section is wider compared to the same layer along 59°S section.

The vertical and horizontal distributions of physical parameters exhibit features characteristic of southern summer. The study area is situated to the south of the Antarctic Polar Front. The three watermasses present in this region are the Antarctic Surface Watermass (ASW), Circumpolar Deep Watermass (CDW) and Antarctic Bottom Watermass (ABW)[1]. During summer, ASW is recognizable as a relatively fresh, highly variable layer above a seasonal halocline, characteristics indicative of the summer heating and melting that leads to its formation (termed as Summer Surface Watermass, SSW). Below the highly variable SSW and above the CDW lies a temperature minimum layer that is the remnant of winter time convection, termed as Antarctic Winter Water (AWW)[14]. The presence of winter water is noticed in the 50 to 150 m depth layer with several gyral cells.

The vertical thermal and salinity structures, particularly on the western side, along 61°S show prominent

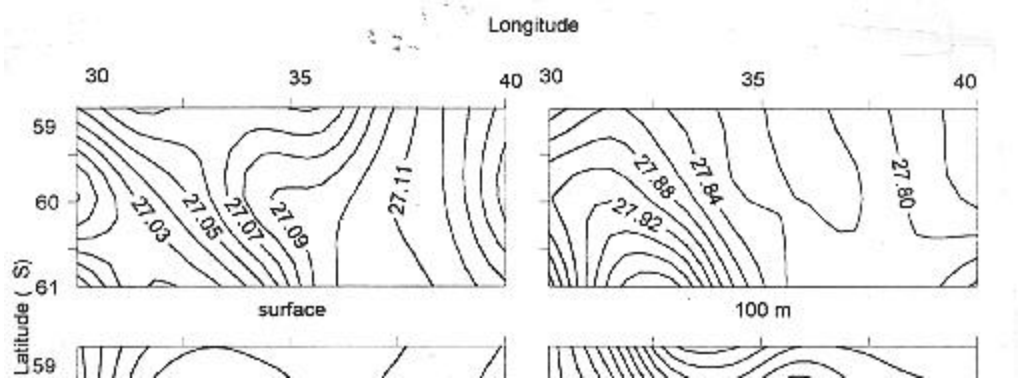

Figure 3 *c*. Spatial distribution of density (σ_t) (kg m^{-3}).

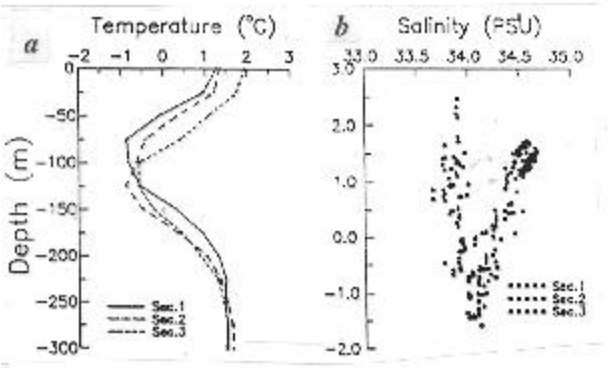

Figure 4. *a*, Mean vertical temperature profiles; *b*, T–S scatter plot.

features indicative of strong divergence where the isolines below the surface are lifted up. The observed spatial variation is due to the variable intensity of the prevailing currents and the consequent mixing of water in the region between the east and west drifts which is usually accompanied by geostrophic upwelling rather than the Ekman divergence. Some studies[15–17] revealed a street of cyclonic eddies in the Indian Ocean sector of the Antarctic Divergence. The effect of the edge of recirculating Weddell Sea water gyre[18] can give rise to the upward tilt of isolines centred at 34°E in the vertical sections along 61°S.

Although DO shows high values in the upper 100 m layer with a gradual decrease below, few higher values are observed in the subsurface within 50–100 m layer (Figure 5*a*). This feature is similar to that of temperature which reflects the influence of winter convection and is attributed to AWW. However, the shoaling of isolines from deeper layers along 61°S between 33 and 34°E could be attributed to the influence of Antarctic Divergence. Along the three sections, DO shows significant vertical variations (Figure 5*a*). The surface layer (0–50 m) has high concentrations of DO (~8.00 ml l^{-1}) which increases further (>8.50 ml l^{-1}) in the subsurface layer (50–75 m), gradually decreasing to about 4.0 ml/l at 300 m. A general increase of DO towards the east is observed in the surface layer along all the 3 sections. Along Section 1, the isolines shoal upwards around 33°E from deeper layers bringing water with lower DO toward the surface layer. This is similar to the divergence trend observed in temperature and salinity fields. Along Sections 2 and 3, the contours appear to converge towards the western and eastern ends and spread in a vertical direction at the centre.

The distributions of major elements show significant variations in the horizontal direction compared to their variations in the vertical (Figure 5*b*–*d*). Strong horizontal gradients of Ca and Mg are noticeable along Section 1 between 33 and 34°E and along Section 2 between 38 and 39°E (Figure 5*b* and *c*). In general, the concentrations of Ca and Mg are higher along Section 2 with an average of 403.33 mg kg^{-1} Ca and 1272.23 mg kg^{-1} Mg compared to the other two sections. Section 3 shows lowest concentrations of these elements with an average of 401.54 mg kg^{-1} Ca and 1267.2 mg kg^{-1} Mg. The vertical variations, however, show an apparent increase of Ca and Mg with depth. Boron presents an inverse trend with low concentrations along Section 2 with an average

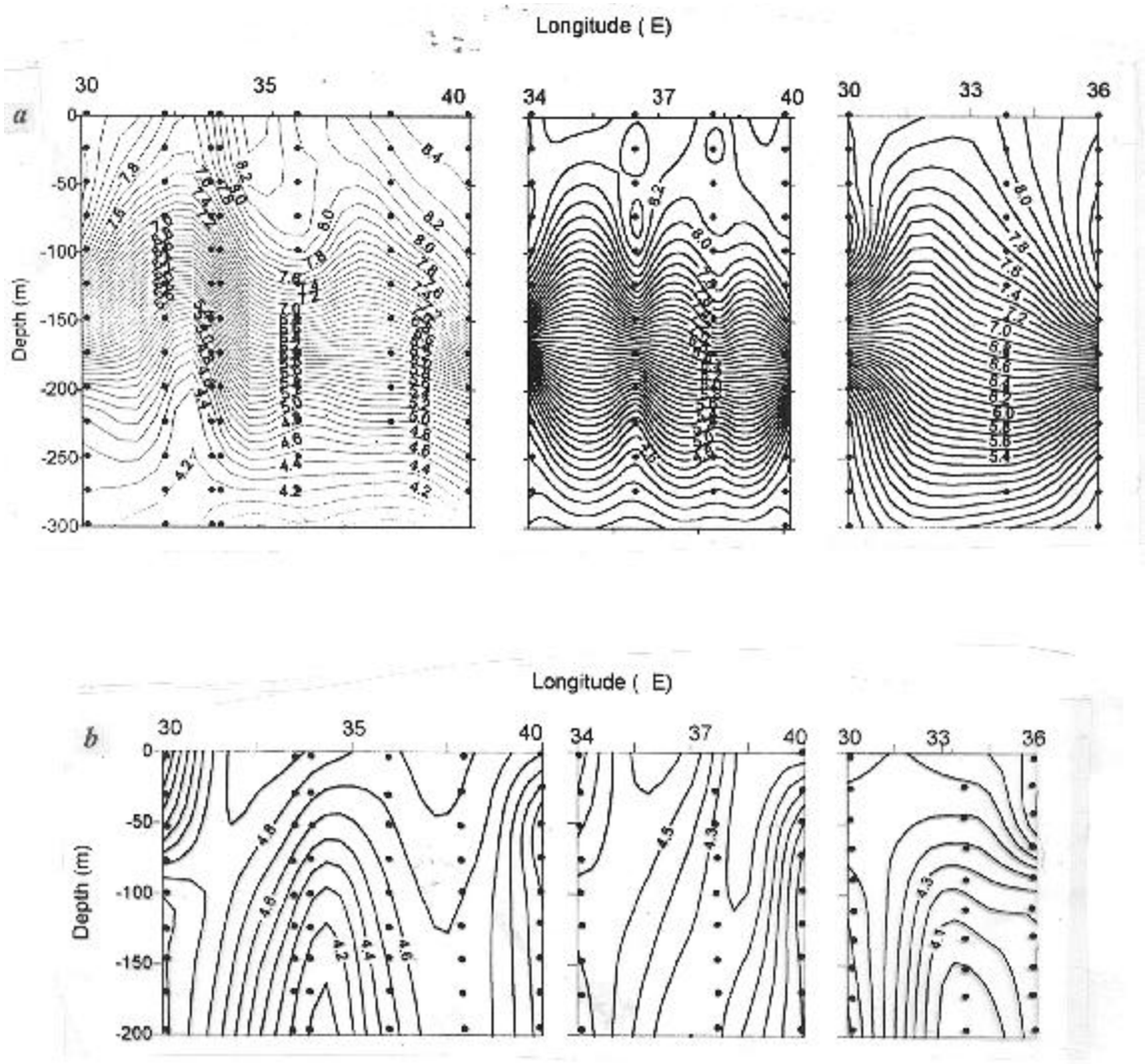

Figure 5 *a*, *b*. Vertical sections along 61, 60 and 59°S of *a*, Dissolved oxygen (ml l^{-1}); *b*, Boron (mg kg^{-1}).

of 4.34 mg kg^{-1} and high concentrations along Section 1 with an average of 4.58 mg kg^{-1} (Figure 5 *d*). A pocket of high boron (~4.5 mg kg^{-1}) is observed at 36 and 37°E along Section 2. Strong eastward gradients are observed at 40°E along Section 1 and at 37 and 40°E along Section 2. Although the vertical gradients in Ca, Mg and B concentrations are weak, the influence of deep upwelled water is evident from the upward tilting of contours in the deeper layer which causes an increase in the concentrations of Ca and Mg and a decrease in that of B relative to the surface and subsurface layers.

The element to chlorinity ratios indicate variations along all 3 sections. However, the variations are more prominent along Section 1 where Ca/Cl varies from 0.02131 to 0.02142 (av. 0.02137) and Mg/Cl varies from 0.06636 to 0.06779 (av. 0.06728). The other two sections show variations in these ratios and the average values for Ca/Cl and Mg/Cl are 0.02130 and 0.06731 along Section 2, and 0.02132 and 0.06736 along Section 3, respectively.

The major elements, Ca and Mg, exhibit spatial variations and indicate a southward increase as evident from their ranges of concentration. The ranges for Mg are 1250.8–1311 mg kg^{-1} along 61°S; 1259–1306 mg kg^{-1} along 60°S and 1260–1284.5 mg kg^{-1} along 59°S. In the case of Ca, the concentrations also show the same kind of variation. The variations of Ca and Mg as observed from

their ratios to chlorinity indicate higher Ca/Cl ratio along 61°S (av. 0.2137) followed by 0.0213 along 60°S and 0.0213 along 59°S. All these ratios appear to be

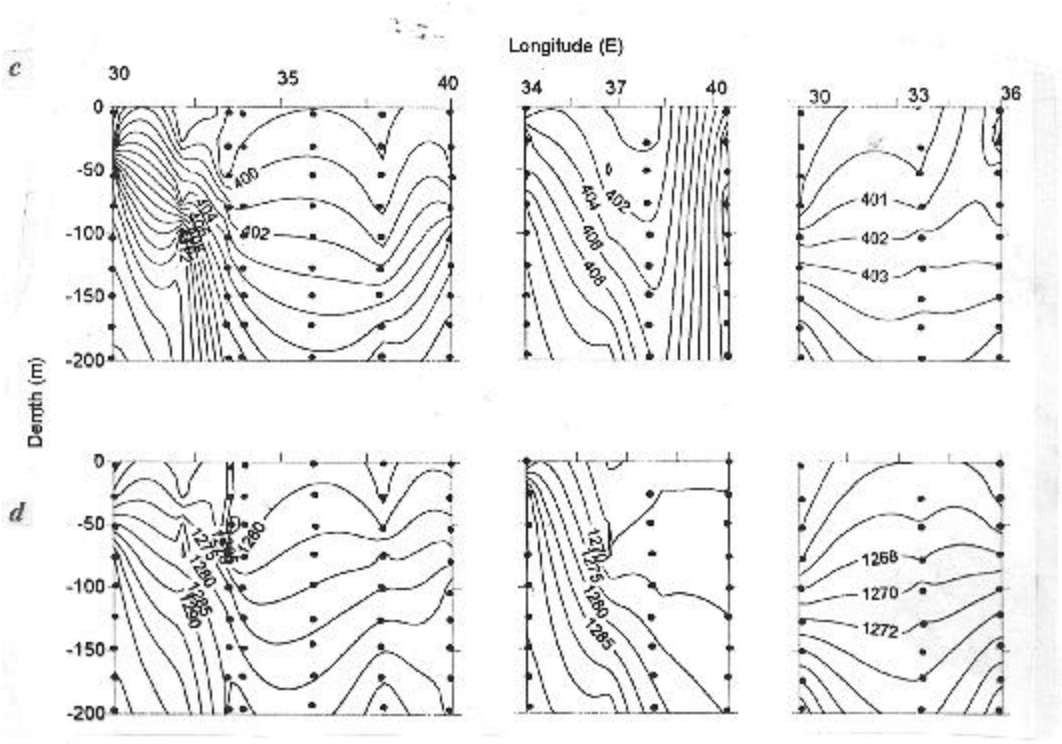

Figure 5 *c*, *d*. Vertical sections along 61, 60 and 59°S of *c*, Calcium (mg kg^{-1}); and *d*, Magnesium (mg kg^{-1}).

higher when compared with the average Ca/Cl ratio (0.02126) for normal sea water[10]. The Ca/Cl ratios in the study region indicate increase in Ca which is possible only due to the addition of Ca to these waters. Ca is biogeochemically active and hence its increase could be attributed to the release of Ca from the calcareous material of the dead planktonic cells in this highly productive region.

Though Mg shows an increase towards south, significant variability is not observed in its ratio to chlorinity along these sections. The average Mg/Cl ratio is found to be 0.06732 which is closer to the normal sea water ratio (0.0668) (ref. 19). However, strong gradients seen at 60°S, 33°E are due to the influence of Antarctic Divergence. Similar features were reported earlier[20] in the ice edge and offshore regions of Antarctica.

Boron shows highest average concentrations along 61°S (av. 4.58 mg kg^{-1}) compared to the sections along 60°S (av. 4.34 mg kg^{-1}) and 59°S (av. 4.48 mg kg^{-1}). This trend of variation of B does not reveal a clear southward increase but, it is reciprocal to that of phytoplankton distribution pattern (Figure 6 *a* and *b*). It is also opposite to Ca and Mg distributions to some extent (Figure 4 *a* and *b*).

The trend of variation observed for boron is also shown by B/Cl ratios along the three sections, which show highest average ratio of 0.242 ´ 10^{-3} along 61°S followed by 0.231 ´ 10^{-3} and 0.239 ´ 10^{-3} along 60 and 59°S, respectively, as against the normal sea water ratio of 0.232 ´ 10^{-3}. This indicates a non-conservative behaviour of boron in the region of investigation, more specifically with addition of boron along 61 and 59°S.

In the open sea, the behaviour of boron is conservative where B/Cl ratio is normal. Any variation in this ratio gives rise to a non-conservative behaviour of boron which is possible only if it is either added or removed from water. In the present study area, the only source of boron addition appears to be

biogenic. Boron is involved in biogeochemical processes and acts as a micro-nutrient for the growth of the phytoplankton. Its biogenic assimilation therefore is related to the productivity of water. The region of study is highly productive where the rate of grazing is expected to be very high. This leads to the release of biogenic boron through organic matter degradation of the dead planktonic cells. However, the contribution by biological materials alone is not very significant to account for such values of boron in these waters. It can therefore be attributed partly to other factors such as watermasses, frontal features and circulation patterns in the region of investigation.

The spatial distributions of phytoplankton and zooplankton are plotted in Figure 6 *a* and *b*, respec-

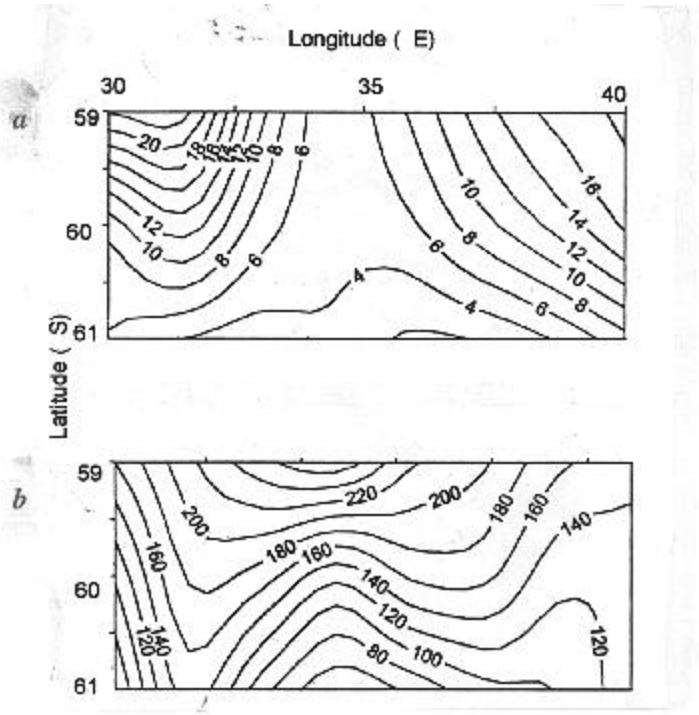

Figure 6. Spatial distribution of *a*, phytoplankton (× 10^3 cell counts per litre), and *b*, zooplankton (ml per 100 m^{-3}).

tively. Phytoplankton blooms are seen along the entire study area. Phytoplankton cell counts in surface waters ranged from 1.92 ´ 10^4 to 2.2 ´ 10^5 cells/litre. Phytoplankton flora consisted of 33 species, 32 diatoms and one dinoflagellate. *Chaetoceros* and *Nitzschia* species dominated. The other common species that prevailed during the study were *Navicula*, *Rhizosolenia*, *Leptocylindrus* and *Corethron Criophilium*. A calm sea state prevailed during 27 January–11 February and was coincident with a bloom of *Chaetoceros* and *Navicula*. At a few stations, inverse relationship of phytoplankton with zooplankton standing stock was observed whereas at rest of the stations values of both these parameters showed similar increasing and decreasing trends. At one of the stations, a 100% trawl catch was observed where drastic fall in both phytoplankton and zooplankton biomass was evident. This confirms the fact that krill feeds actively on phytoplankton as well as zooplankton.

The distribution, abundance and species composition of zooplankton were also studied. Zooplankton biomass ranged from 9.79 to 303.62 ml 100 m^{-3} (x = 142.14 ± 77.02). A total number of 14 different taxa were recorded with *copepods*, *chaetognaths*, *euphausiids* and *salps* being the dominant ones. *Copepods* formed the major constituent of zooplankton community and comprised more than 70% of the zooplankton catch. Swarms of krill and *salps* were observed during the study period which were the prime cause for the high standing stock of zooplankton. The *euphausiids*, particularly the Antarctic krill, *Euphausia superba*, were found in great abundance in both adult and larval stages during the present study. They occurred along all 3 sections with a peak density of 815 100 m^{-3}.

The calm sea state which prevailed during the study period favoured proliferation of certain phytoplankton species to bloom condition[21]. The phytoplankton cell counts in surface waters was quite high (Figure 6). These cells represent 33 species consisting of 32 diatom and one dinoflagellate. *Chaetceros*, *Flagelaria* and *Nitzschia* dominated the phytoplankton biomass. Other common species that prevailed were *Navicula*, *Rizosolenea*, *Leptocylindrus* and *Corethron criophilun*. The regions where the phytoplankton population in the oceanic waters are dominated by nanoplankton forms and high nutrient content favour the growth of these organisms[22]. The high concentration of nutrients along with phytoplankton blooms observed in the present investigation substantiate the above study.

Conclusion

The prevailing physico-chemical conditions in the study region appear to strongly influence the availability of food to zooplankton. The Antarctic waters have a significantly higher standing crop of zooplankton than the tropical and temperate regions, with a peak during the summer season[23]. High standing stock and higher biomass values of zooplankton are observed in the study region during the observation period. While some phytoplankton losses occur in the ocean via sinking, the vast majority of cells disappear by zooplankton grazing. Zooplankton grazing exerts a more consistent controlling influence on phytoplankton abundance in the open ocean. Therefore, the mesozooplankton heterotrophy is an important link in the rapid regeneration and release of nutrients.

---

1. Deacon, G. E. R., *Discovery Rep.*, 1937, **15**, 124.
1. Mackintosh, N. A., *Discovery Rep.*, 1946, **23**, 177–212.
2. Jacobs, S. S. and Georgi, D. T., *Deep Sea Res.* (Supplement) 1977, **24**, 43–84.
3. Taylor, H. W., Gordon, A. L. and Molinelli, E., *J. Geophys. Res*., 1978, **83**, 4572–4578.
4. Deacon, G. E. R., *Deep Sea Res*., 1982, **29**, 1–15.
5. Lutjeharms, J. R. E. and Valentine, H. R., *Deep Sea Res*., 1984, **31**, 1461–1475.
6. Lutjeharms, J. R. E., *Deep Sea Res*., 1985, **32**, 1499–1509.
7. Naeije, M. C., Wisse, E., Scharrooo, R. and Wakker, K. F., Proceedings of the 2nd ERS-1 Symposium, Hamburg, 1993.
8. Webb, D. J., De Cuevas, B. A., Killworth, P. D. and Rowe, M., Internal Doc. 293, IOS., Wormley, England, 1990, p. 14.
9. Culkin, F. and Cox, R. A., *Deep Sea Res*., 1966, **13**, 789–804.
10. Hatcher, J. T. and Wilcox, L. V., *Chem*., 1970, **22**, 567–569.
11.
12. Veronis, G., *J. Mar. Res.*, 1972, **30**, 255–277.
13. Murty, V. S. N., Sarma, Y. V. B., Murty, C. S. and Rao, D. P., *J. Mar. Res.*, 1992, **50**, 207–228.
14. Mosby, H., *The Waters of the Antarctic Ocean – Scientific Results of the Norwegian Antarctic Expeditions, 1927–1928*, 1934, vol. 1, p. 131.
15. Ivanov Yu, A., *Okeanol. Issled.*, 1961, **3**, 30–51.
16. Zverev, A. A., *Tr. Sov. Antark. Eksped.*, 1963, vol. 17, pp. 144–155.
17. Wakatsuchi, M., Ohshima, K. I., Hishida, M. and Naganobu, M., *J. Geophys. Res*., 1994, **99**, 20417–20426.
18. Gordon, A. and Molinalli, E., *Southern Ocean Atlas: Thermohaline and Chemical Distribution*, Columbia Univ., Press, New York, 1982, p. 33.
19. Carpenter, J. H. and Manella, M. E., *J. Geophys. Res*., 1973, **78**, 3621–3626.
20. Shirodkar, P. V., Alagarswamy, R., Goes, J. I. and Fondekar, S. P., *Polar Rec.*, 1992, **28**, 127–136.
21. Verlencar, X. N., Vijayakumar, R., Flory, S. and Linette, M., *Fish. Technol.* (in press).
22. Verlencar, X. N., Somasundar, K. and Qasim, S. Z., *Mar. Ecol. Prog. Sci*., 1990, **61**, 41–59.
23. Foxton, P., *Discovery Rep.*, 1956, **28**, 193–235.

ACKNOWLEDGEMENTS. We thank the Director NIO, for his keen interest in this study. We are grateful to the Department of Ocean Development, Government of India for FORV *Sagar Sampada* Expedition. Thanks are also due to Dr V. S. N. Murty for his suggestions during the preparation of this manuscript.

Received 6 February 1999; revised accepted 4 October 1999